Journal of Statistical Physics, Vol. 119, Nos. 3/4, May 2005 (© 2005)
DOI: 10.1007/s10955-005-4427-9

Effects of Field Orientation on the Driven Lattice Gas

Paul D. Siders[1]

Received February 6, 2004; accepted January 21, 2005

Steady states of the driven lattice gas (DLG) on triangular, hexagonal and square lattices with the field at several fixed orientations to the principal lattice vectors were studied by Monte Carlo simulation. In most cases a strong field suppressed change to a low-temperature ordered phase. On each lattice, one field orientation that caused nonequilibrium ordering was identified. On triangular and hexagonal lattices, dependence of energy and anisotropy on field strength was studied at those orientations. Anisotropic ordering along the field developed at intermediate temperatures under weak fields. Partial ordering along the field persisted to low temperature under strong fields.

KEY WORDS: Driven lattice gas; Monte Carlo; hexagonal lattice; triangular lattice.

1. INTRODUCTION

The two-dimensional driven lattice gas (DLG) was defined for a square lattice with the driving field parallel to one of the lattice vectors.[1,2] Properties of the DLG are described in recent books and reviews.[3–5] A striking feature of the DLG is that a strong field raises the critical temperature 40% above the equilibrium lattice gas critical temperature. In the equilibrium lattice gas on half-filled finite lattices with periodic boundary conditions phase boundaries orient along lattice vectors, but in the DLG phase boundaries parallel the field. Anisotropy due to the field is a key feature of the DLG. Nearest-neighbor interactions on the square lattice parallel the lattice vectors, one half parallel to the field, the other perpendicular. That special arrangement is necessary for the field effects that have been observed.

[1]Department of Chemistry, University of Minnesota Duluth, Duluth, Minnesota 55812; e-mail: psiders@d.umn.edu

The present work uses the Monte Carlo method to find steady states of the DLG on the square lattice with a variety of field-lattice orientations, and on the triangular and hexagonal lattices where lattice vectors are not orthogonal. On the latter lattices, the field can be parallel to one lattice vector without being perpendicular to the other and bond directions need not parallel principal lattice vectors. Eleven combinations of lattices and field directions are studied. With strong fields, anisotropic particle distributions oriented along the field are observed only when the field is perpendicular to a bond direction on the lattice. On the square lattice the critical temperature is clearly elevated by a field that is perpendicular to bonds. Anisotropic low-energy steady states develop over broad temperature ranges on triangular and hexagonal lattices. Clusters oriented along the field form at intermediate temperatures. If the field is strong enough they persist to low temperatures.

On the hexagonal lattice, the temperature and field-strength dependences of energy and orientational ordering depend little on lattice size. For 2×2 and 3×3 lattices, steady state probabilities of particle configurations are calculated by solving the master equation. At low temperatures relatively few configurations are occupied, their probabilities determined by the field strength.

2. MONTE CARLO METHOD

The critical density, lattices half filled, was used in all the simulations reported here. The three lattices' connectivities ($z = 3$, 4 and 6) strongly affect the equilibrium phase transition temperature. Equilibrium values of kT_c/J are 1.52, 2.27, and 3.64 for the hexagonal, square and triangular lattices, respectively.[6] Temperatures reported are scaled by $T_c(0)$. Where temperature is reported as $T/T_c(0)$, $T_c(0)$ is the equilibrium critical temperature for the lattice of the type at hand and of infinite size.

The energy of a configuration was calculated in the usual lattice-gas way: $H = -4J$ times the number of bonds. Boundary conditions were periodic (toroidal). To calculate a hopping rate, the energy change of a hop was combined with the dot product of the field and the proposed hop: $\Delta E_{\text{hop}} = \Delta H_{\text{hop}} - E \cdot (\text{hop})$. Hopping rates were calculated with the Metropolis rate function, $\Phi(\Delta E_{\text{hop}}) = \min\{1, \exp(-\Delta E_{\text{hop}}/(kT))\}$.

Most Monte Carlo simulations were run on serial computers. Serial random number generators used were simple congruential, shuffled congruential and lagged Fibonacci generators[7] for generating initial configurations, for accepting transitions, and for choosing neighbor sites for possible hops. As a check of the generators, some runs were repeated with other generators.[8] No significant differences were found. Most

calculations on larger lattices were done in parallel mode (by the "embarrassingly parallel" method of dividing runs among nodes) using the LAM message passing interface[9] and the additive lagged Fibonacci generator in the SPRNG[10] library of random number generators.

For a particular temperature, field and lattice, a typical calculation averaged the results of 16 runs, each of which discarded 10^7 equilibration steps and then collected data at intervals of 10^3 steps for 10^6 steps. Some conditions required more and longer runs. Reported data used enough runs and steps so that the rate of change of energy with respect to steps, estimated by linear regression, was less than twice the estimated standard deviation in the rate of change of energy. That is, energy appeared to have reached steady state in the data that are reported. Every run was started from a randomly filled lattice so individual runs were independent of one another whether at the same or different temperatures. Specially prepared non-random initial configurations were used to test single-strip stability in a few cases.

For square lattices, the average of the anisotropy parameter m[2–4] was calculated. Parameter $m = (M_{||}^2 - M_{\perp}^2)^{1/2}$, where (ref. 3, Eq. (4.5)) $M_{\perp}$ ($M_{||}$) is the average of the magnetization squared in strips perpendicular (parallel) to the field direction, divided by the number of sites on the lattice.

$$M_{\perp}^2 = L_{\parallel}^{-1} \sum_{\parallel \text{sites}} \left(L_{\perp}^{-1} \sum_{\perp \text{sites}} (2n_{\text{site}} - 1) \right)^2 \tag{1}$$

The structure factor,[11] which is readily applied to arbitrary field orientations, was calculated for all lattices and field orientations.

The three lattices' unit cells and the field orientations considered appear in Fig. 1. Square and triangular cells are singly occupied; hexagonal doubly. Nearest-neighbor bond directions are shown. Cell dimensions for the lattices were chosen so that the nearest-neighbor distance ("bond length") was unity on all lattices. After an initial study of lattice size dependence, routine calculations used 24×24 hexagonal lattices (576 particles) and 32×32 square and triangular lattices (512 particles). Infinite-field calculations were repeated with 48×48 hexagonal and 64×64 triangular lattices.

A field strength $|E| = 15kT$ (or simply 15 when kT is incorporated in E) has been used as a saturating field.[2,4,12,13] That is suitable for temperatures larger than or on the order of $T_c(0)$. The field orientations considered in this work required calculations both near $T_c(0)$ and at much lower temperature. If ε/kT is fixed at 15, where ε is the magnitude of the field, then when kT/J falls below about 0.3 the field becomes irrelevant compared to bond energies and the system simply freezes rapidly. To keep the field dominant to low temperature, the present work used

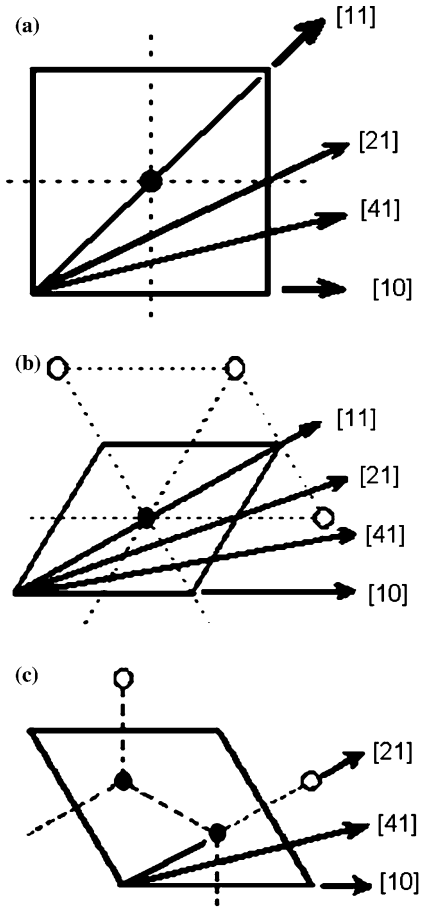

Fig. 1. Unit cells and field orientations on the (a) square, (b) triangular, and (c) hexagonal lattices. Dashed lines show connectivity to nearest neighbors. Open circles are some of the nearest neighbor sites.

$\varepsilon = 15Jz$ as the saturating field. Some calculations were done with an infinite field, in which case hops against (with) the field were forbidden (accepted) and the usual rate function was used for hops orthogonal to the field. Figure 2 shows $\langle U/(Jz)\rangle$ for a square lattice with the field parallel to [11], to compare the results of an infinite field and of using $15kT$ and $15Jz$ for ε. When T falls below $(1/3)T_c(0)$ then for $\varepsilon = 15kT$ the system freezes rapidly, as would be expected for ΔH_{hop} dominating $E \cdot \text{hop}$ in ΔE_{hop}. If one uses $\varepsilon = 15kT$, none of the systems studied in this paper remains disordered below about $T/T_c(0) = 0.2$, at which temperature $15kT$

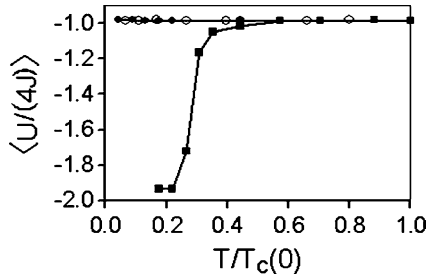

Fig. 2. Comparison of the effect of field magnitudes (•) $15Jz$, (○) infinite, and (■) $15kT$, for a field parallel to [11] on a 32×32 square lattice.

approximately equals $1.5Jz$. As Fig. 2 indicates, a field of magnitude $15Jz$ is saturating, effectively infinite at all temperatures.

3. SQUARE LATTICE

Figure 3 shows the steady-state energy calculated on a 32×32 square lattice. The field magnitude is $15Jz$. For the [10] orientation, infinite-field results are also shown and are the same as for $15Jz$. The customary field orientation [10] yields the customary phase transition. Scaling analysis of $\ln(m)$ *vs.* $\ln|T/T_c(0) - T_c(E)/T_c(0)|$ yields $T_c/T_c(0) = 1.38$, in approximate agreement with earlier results.[4,13] With the field along [10], the energy approaches $-2Jz$ at low temperature, as expected in a condensed state, and tends toward $-Jz$ at high temperature, as expected for a completely disordered state.

The three other field orientations studied on the square lattice, [11], [21] and [41], show no evidence of a phase transition. For those

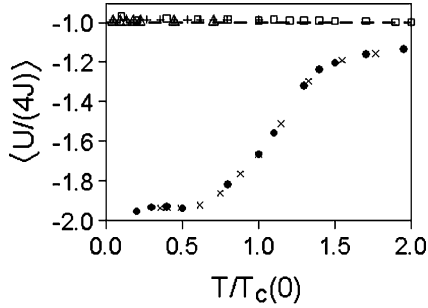

Fig. 3. Energy on the square lattice with saturating field oriented along (•, ×) [10], (□) [41], (+) [21] and (Δ) [11]. Field strength is $15Jz$ except (×) indicates infinite field.

orientations, the energy remains near $-Jz$ down to the lowest temperature used. For the [11] orientation the asymmetry parameter m was equal to 0.06, much less than unity, at all temperatures. The maximum of the structure factor was less than 0.4 at all temperatures and moreover occurred at short wavelengths. This lack of orientational order is consistent with Katz et al., 1984 statement[2] that nontrivial temperature dependence under an infinite field is possible only for [10] and [01] field directions.

4. TRIANGULAR LATTICE

Energies on a triangular lattice are shown in Fig. 4 for saturating fields. As on the square lattice, only one of the tested orientations shows nonequilibrium anisotropic order. That orientation, [11], is perpendicular to bonds so rates of hops along $[1, -1]$ bonds are just as under zero field. Fields of all other orientations drive hops along all bonds, leaving no field-free lines of bonds. When the field parallels [11] then energy decreases as ordering increases with decreasing temperature, down to $T/T_c(0) = 0.08$. The two runs with $T/T_c(0) < 0.08$ showed no further energy drop. Figures 5 and 6 show single 64×64 configurations at the lowest and highest temperatures studied, respectively. The apparent disorder in the low-temperature configuration is consistent with the average energy at that temperature, $-1.37Jz$, much above the energy $-2Jz$ of a one-strip totally ordered configuration. Energies under a saturating [11] field depend strongly on system size. A strong field tends to disrupt order, selecting configurations that are only partially ordered along the field direction, better ordered as the system size increases. The present data and computational methods are inadequate to address whether, on an infinite lattice,

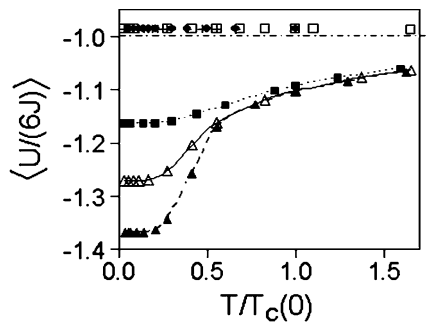

Fig. 4. Energy on the triangular lattice with field strength $15Jz$ and field orientations (•) [10], (□) [41], (+) [21] and (Δ, ▲, ■) [11]. Lattices are 32×32 except (▲) 64×64 and (■) 16×16.

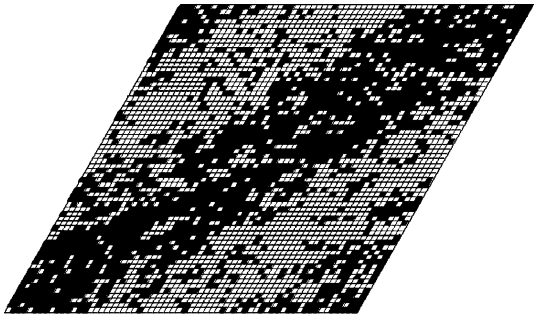

Fig. 5. Configuration at $T/T_c(0) = 0.03$ on the 64×64 triangular lattice with infinite [11] field.

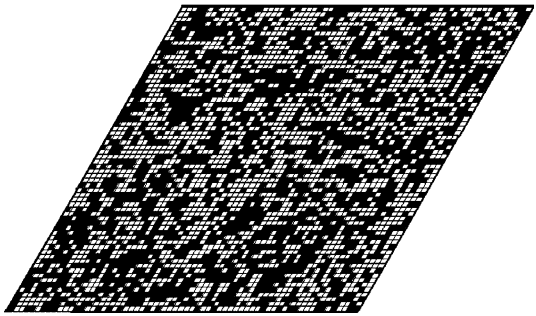

Fig. 6. Configuration at $T/T_c(0) = 5.90$ on the 64×64 triangular lattice with infinite [11] field.

the low-temperature high-field configurations would reach the minimum energy $\langle U \rangle = -2Jz$.

Figures 7 and 8 show the effect of increasing field strength on the energy and structure factor $S(1, -1)$, on 32×32 triangular lattices. At low field strengths and intermediate temperatures configurations align with the field, as indicated by energy curvature changes, corresponding to heat capacity maxima, and structure factor maxima for field strengths $3J$ and $6J$. At those fields, the system loses its alignment with the field at lower temperatures and freezes into fully ordered states. Increasing field strength, at least at these lattice sizes, disperses the intermediate-temperature alignment and prevents full order at low temperature. The change of field effect occurs for ε between $6J$ and $12J$.

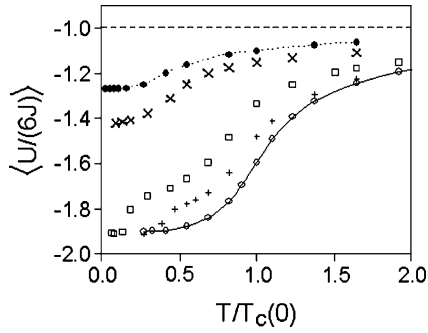

Fig. 7. Dependence of energy on magnitude of a field directed along 32×32 triangular lattice [11]. Values of ε: (○) 0, (+) $3J$, (□) $6J$, (×) $12J$, and (•) $15Jz = 90J$.

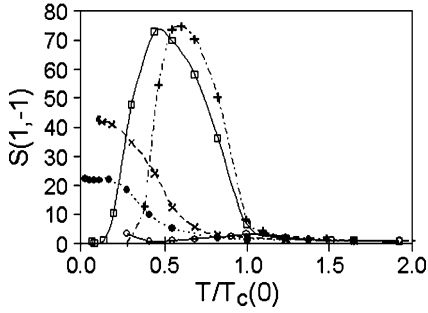

Fig. 8. Dependence of $S(1, -1)$ on magnitude of a field directed along 32×32 triangular lattice [11]. Symbols as in Fig. 7. Lines are drawn merely to help distinguish the data sets.

5. HEXAGONAL LATTICE

Three field directions, [10], [41] and [21], were tested on the hexagonal lattice. (Direction [11] is not listed because it is equivalent to [10].) Figure 9 shows the saturating field in [41] and [21] directions completely suppressing the equilibrium phase transition. The [10] field, which is perpendicular to a bond direction, does cause partial ordering in the field direction. (Results of both infinite and $15Jz$ [10] fields are shown and are the same.) The slope of the energy is largest at $T/T_c(0) \approx 1.2$. As on the triangular lattice, anisotropic ordering increases gradually over a wide temperature range and does not reach a fully ordered state at the lowest temperatures used. The data shown are from runs that started from randomly filled lattices. Runs that start from a single strip along [10] are stable for 10^7 or more Monte Carlo steps but eventually break up to a less ordered state. Data from 24×24, 32×32 and 48×48 lattices show

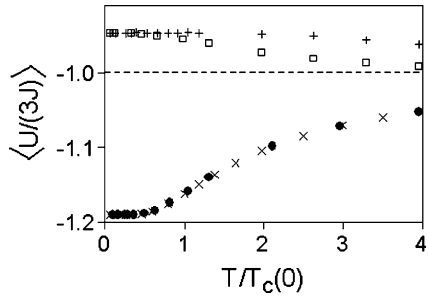

Fig. 9. Energy on the 24×24 hexagonal lattice with saturating field oriented along (•) [10], (□) [41] and (+) [21]. Data are for $\varepsilon = 15Jz$ except (×) infinite field.

the same gradual energy decrease, Fig. 10, suggesting that the temperature dependence shown is not the result of small lattice size.

For an infinite [10] field, Fig. 11 shows values of the structure factor, indicating partial ordering along [10]. The structure factor $S(k_1, k_2)$ has a line of maxima along $k_1 = 0$. $S(0, 1)$, $S(0, 3)$ and $S(0, 6)$ are shown in the figure. Other values of $S(0, k_2)$, for $0 < k_2 < 16$, are similar. Evidently there is partial alignment with the field. Unlike the triangular [11] case, there is no single large wavelength associated with that ordering.

The partially ordered state on the hexagonal lattice resembles in some respects the "stringy state" that was observed on a square lattice with anisotropic couplings.[5] There, too, the structure factor transverse to the field was small but nonzero. Zia *et al.*[14] proposed that the low-temperature state on a square lattice "is characterized by multiple strips, with a nontrivial distribution of strip widths." The low-temperature ordering on the hexagonal lattice may be a sort of stringy state.

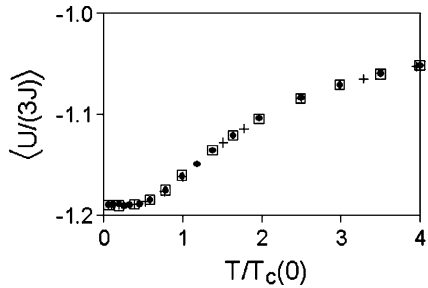

Fig. 10. Dependence of energy on hexagonal lattice size under [10] saturating field. (•) 24×24, (□) 32×32, (+) 48×48 unit cells.

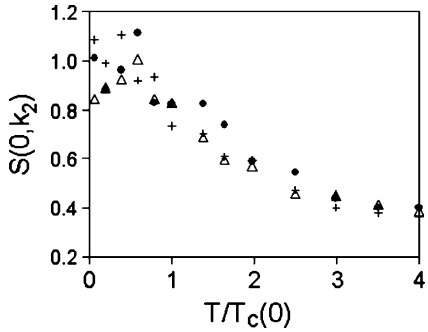

Fig. 11. Structure factor $S(0, k_2)$ on the 32×32 hexagonal lattice with field $15Jz$ along [10]. $k_2 = (\bullet)$ 1, (Δ) 3, and $(+)$ 6.

The transition from a low-energy to a higher-energy low-temperature state occurs at a field strength near $8J$, as shown in Fig. 12, and much as seen on triangular lattices. Fields with $\varepsilon \geqslant 12J$ reproduce the infinite-field results. Structure factor $S(0,1)$, reflecting ordering along the [10] field, is plotted in Fig. 13 for several field strengths. Zero field leads to an isotropic mix of solid configurations for which the average $S(0, 1)$, $S(1, 0)$ and $S(1, -1)$ are all large and equal. A weak field, $\varepsilon = 3J$, leads to enhanced order along the field at intermediate temperatures, peaking near $T/T_c(0) = 0.6$. Stronger fields, $\varepsilon = 6J$ and $8J$, move along-field ordering to lower temperatures and preserve it to the lowest temperatures simulated, at which single-strip configurations along the field are stable. Still stronger fields, $9J$ and higher, suppress single-strip ordering along the field, yielding the situation for which structure factors are shown in Fig. 11.

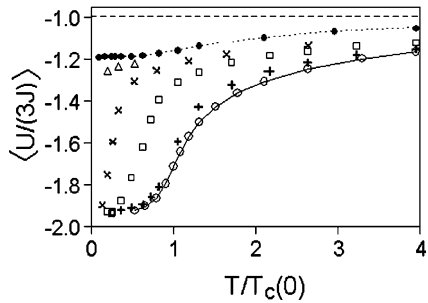

Fig. 12. Dependence of 24 × 24 hexagonal-lattice energy on magnitude of a [10] field. Values of ε: $(\circ)$ 0, $(+)$ $3J$, $(\square)$ $6J$, $(\times)$ 8J, (Δ) 9J, and $(\bullet)$ infinity.

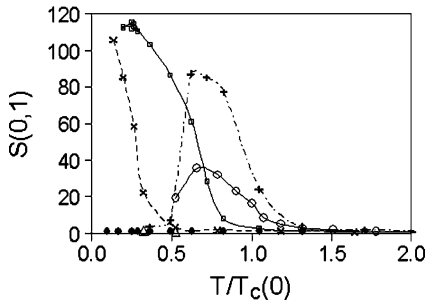

Fig. 13. Dependence of $S(0, 1)$ on magnitude of a field directed along 24×24 hexagonal lattice [10]. Symbols as in Fig. 12. Lines are drawn merely to help distinguish the data sets.

6. PAIR MEAN FIELD THEORY

Pair-level mean field theories of the DLG on the square lattice, with the field parallel to a lattice vector, have been presented by Dickman,[15] Pesheva[16,17] and others. The pair mean-field theories focus on clusters of two lattice sites plus their immediate neighbors. Steady-state probabilities of cluster configurations are expressed in terms of one- and two-site densities. The pair density functions are steady-state solutions of master equations. In Dickman's method the critical temperature is located by finding the low-temperature limit of stability of solutions with respect to density fluctuation perpendicular to the field. Pesheva's maximum entropy method postulates a form for the entropy as a function of density, then locates coexisting phases through entropy maxima. At zero field, both theories yield the Bethe-Peierls mean field critical temperature $T_c(0) = 2.885J/k$. Both theories successfully predict T_c to be an increasing function of field strength. Dickman's and Pesheva's pair mean field theories give 3.21 and 3.32, respectively, for $kT_c(\infty)/J$.

The pair mean field theories of Dickman and Pesheva were generalized to triangular and hexagonal lattices by using three clusters, one along each bond direction on the lattice. A cluster consists of two central sites plus their nearest neighbor sites. Figure 14 shows one cluster on the triangular lattice and one on the hexagonal lattice. The number of sites (central plus neighbors), $n$sites, equals 10, 8 and 6 on the triangular, square and hexagonal lattices, respectively. Arbitrary orientations of the field are allowed. The rate function for transitions is the same as that used in the Monte Carlo calculations.

Pair density functions are b_k, the probability of a hole adjacent to a particle along the kth bond direction, and w_k and z_k, the probabilities of adjacent vacancies and particles, respectively, along bond direction k. On

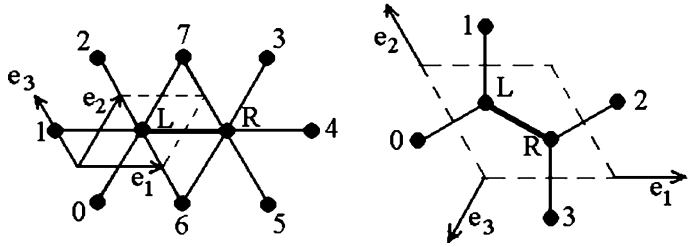

Fig. 14. One of three clusters on the triangular lattice (left) and the hexagonal lattice (right). The central (L,R) pair, neighbor sites (numbered), unit cells and unit vectors are shown.

the triangular lattice, bond direction k is along unit vector e_k. On the hexagonal lattice, bond 1 is along $e_1 - e_2$, bond 2 along $e_1 + e_2$, and bond 3 is along $-2e_1 - e_2$. Singlet density ρ and the b_k suffice to determine w_k and z_k because $w_k = 1 - \rho - b_k$ and $z_k = \rho - b_k$. The probability of a particular configuration, or occupancy, α on cluster k is $P_\alpha^{(k)}$ where k runs from 1 to n_c ($n_c = 2$ for the square lattice, 3 for triangular and hexagonal lattices) and α runs over all possible occupations of the cluster's sites. Configuration probabilities are calculated in terms of singlet and pair probabilities as discussed in detail by both Dickman and Pesheva for the square lattice. On the triangular lattice the probability of a 10-site configuration is, in terms of pair and singlet densities, $\rho^{(10)}(\mathrm{L}, \mathrm{R}, 0, \ldots, 7) = \rho^{(2)}(\mathrm{L}, \mathrm{R})\rho^{(2)}(0, \mathrm{L})\rho^{(2)}(1, \mathrm{L})\rho^{(2)}(2, \mathrm{L})\rho^{(2)}(3, \mathrm{R})\rho^{(2)}(4, \mathrm{R})\rho^{(2)}(5, \mathrm{R})\rho^{(2)}(6, \mathrm{R})\rho^{(2)}(7, \mathrm{L})/[\rho^{(1)}(\mathrm{L})\rho^{(1)}(\mathrm{R})]^4$. The sites are labeled (L,R) and numbered (0–7) as in Fig. 14. Pair density $\rho^{(2)}(i, j)$ is one of the $\{b_k, w_k, z_k\}$, depending on the occupancy and orientation of sites i and j. Likewise, $\rho^{(1)}(i)$ equals either ρ or $(1 - \rho)$, depending on the occupancy of site i. The hexagonal lattice has only six sites per cluster, and its configuration probability is $\rho^{(6)}(1, 2, \ldots, 6) = \rho^{(2)}(\mathrm{L}, \mathrm{R})\rho^{(2)}(0, \mathrm{L})\rho^{(2)}(1, \mathrm{L})\rho^{(2)}(2, \mathrm{R})\rho^{(2)}(3, \mathrm{R})/[\rho^{(1)}(\mathrm{L})\rho^{(1)}(\mathrm{R})]^2$.

The master equation for b_k has the form

$$\frac{db_k}{dt} = \sum_{j=1}^{n_c} G_k^{(j)}\left(b_1, \ldots, b_{n_c}; \rho, T, \vec{\varepsilon}\right) \tag{2}$$

where $G_k^{(j)}$ is the average change in b_k per hop on the jth cluster, given probabilities b_i and density ρ, which determine $P_\alpha^{(k)}$, and the temperature, field and rate function Φ.

$$G_k^{(j)} = \sum_\alpha \Delta b_k \Phi(\Delta E_{\mathrm{hop},\alpha}^{(j)}) P_\alpha^{(j)} \tag{3}$$

The summation index α runs over $2^{n\text{sites}-1}$ configurations consistent with one particle and one hole in the central pair of the cluster. The argument of the rate function is the same as in Monte Carlo simulation, the energy change plus the dot product of the field and the particle hop. For the results given in this paper Φ is the Metropolis rate function.

Iterative solution of the master equation yields steady-state values of b_k. Extending Pesheva's entropy postulate from the square lattice (with two bond directions) to the triangular and hexagonal lattices (3 bond directions) yields the entropy in terms of ρ and the b_k.

$$S/k_B = c_1[\rho\ln(\rho)+(1-\rho)\ln(1-\rho)] - c_2\sum_{k=1}^{n_c}[z_k\ln(z_k)+2b_k\ln(b_k)+w_k\ln(w_k)] \tag{4}$$

where $(c_1, c_2) = (3, 1)$, (5,1) and (2,1/2) for the square, triangular and hexagonal lattices, respectively, and k_B is Boltzmann's constant. The potential to minimize is proportional to Helmholtz energy, $A/k_B = [U - U(0)]/(k_BT) - S/k_B$, where U is the average energy per site (calculated from the b_k) and $U(0)$ is the limit of U at zero temperature, $-2J\rho z$.

The computational procedure is to choose a density, then calculate the steady-state b_k and then the free energy. That procedure is iterated to find the density, and simultaneously b_k, that minimize the free energy. At low temperature, two densities are found. The two densities approach one half as the temperature increases, merging at the critical temperature.

Critical temperature as a function of field orientation is shown in Fig. 15. The angle θ is the angle between the field and lattice vector e_1. At zero field, the maximum-entropy mean field calculations reproduce the known Bethe pair-mean-field critical temperatures: $kT_c(0)/J = 1.821$ (hexagonal), 2.885 (square) and 4.933 (triangular). The critical temperature on the square lattice and with an infinite field along [10] is $kT_c/J = 3.32$, as found by Pesheva, and so $T_c(\infty)/T_c(0) = 1.15$. On the triangular lattice with the field along [11], i.e. $\theta = 30^\circ, kT_c(\infty)/J = 5.44$, or $T_c(\infty)/T_c(0) = 5.44/4.93 = 1.10$. On the hexagonal lattice with the field along [10], $kT_c(\infty)/T_c(0) = 2.54/1.82 = 1.40$. On all three lattices and for all field orientations and magnitudes, it appears that T_c is bounded below by its pair-mean-field equilibrium value and bounded above by the singlet mean field result $T_c = zJ/k$. This differs from the Monte Carlo result that for most orientations on all three lattices a strong field prevents phase transition. That general behavior is not reproduced even qualitatively by the present mean field theory.

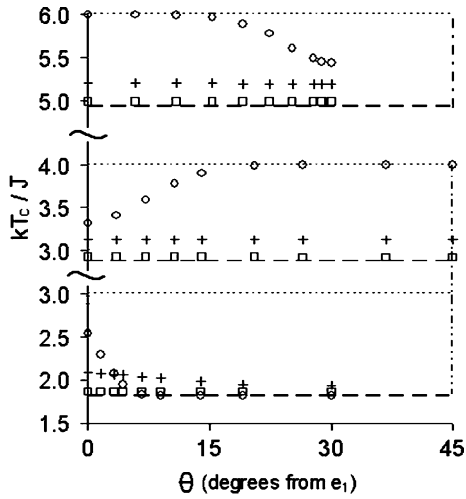

Fig. 15. Maximum-entropy mean field critical temperatures for the triangular (top), square (middle) and hexagonal (bottom) lattices. (- - -) singlet mean field, (— — —) Bethe pair mean field, (□) $\varepsilon = Jz$, (+) $\varepsilon = 2Jz$, (○) $\varepsilon = 15Jz$.

7. SMALL HEXAGONAL LATTICES

Weak size dependence on the hexagonal lattice suggests studying lattices so small that the master equation for configuration probabilities can be solved exactly. The master equation solution was given in detail by Zhang[18,19] for square lattices and extended to triangular lattices and a related hexagonal lattice by Kumaran.[20]

The 2×2 hexagonal lattice's 4 particles on 8 sites assume 70 configurations. With the field oriented along [11] (which is equivalent by symmetry to [10] for hexagonal lattices) three symmetry operations are translation along [10] and [01] and reflection across [11]. Those symmetries divide the configurations into 13 classes so the transition matrix in the master equation is only 13×13. Symbolic algebra (using Mathematica[21]) was used to find exact steady-state probabilities. The energy of this tiny system is shown in Fig. 16. Behavior is similar to that of larger hexagonal lattices except that the low-temperature energy is independent of field strength, not rising to the less-ordered value seen for the larger lattices. Even though the low-temperature energy is independent of field strength the configuration probabilities are not. Two classes, each having 4 bonds, dominate at low temperature. The mix of the two is highly field dependent, as shown in Fig. 17, but because both classes have the same energy the system's energy is field independent at low temperature. A strong field

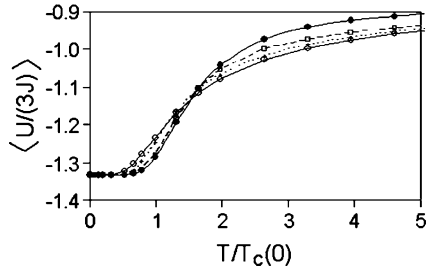

Fig. 16. Energy of 2×2 hexagonal lattice. Values of ε: (○) 0, (–+–) $3J$, (–□–) $6J$, and (•) infinity. Energies were calculated exactly so markers are merely to help distinguish different field strengths.

selects the configurations in which the zig-zag chain of bonds is oriented along the field.

The 3×3 hexagonal lattice's 9 particles on 18 sites divide by symmetry into 2710 classes. The transition matrix, which is sparse, was calculated numerically. From that exact transition matrix steady-state probabilities were calculated by minimizing their time derivatives. As Fig. 18 shows, the 3×3 lattice is large enough that strong fields yield a high-energy disordered state at low temperature, as Monte Carlo simulations showed for larger lattices. Behavior of the structure factor, Fig. 19, is also similar to that on large lattices. Because the field is along [11], $S(1, -1)$ here is equivalent to $S(1, 0)$ from the Monte Carlo simulations. A weak field, $\varepsilon = J$, gives a peak in $S(1, -1)$ at $T/T_c(0) = 0.33$, $kT/J = 0.5$. Slightly stronger fields ($\varepsilon = 3J$ and $6J$ are shown) shift the peak to near-zero temperature. (Unlike the analytical 2×2 solutions, the numerical transition matrix cannot be computed at zero temperature.) Still stronger fields ($\varepsilon = \infty$ is shown) reduce the low-temperature ordering along the field.

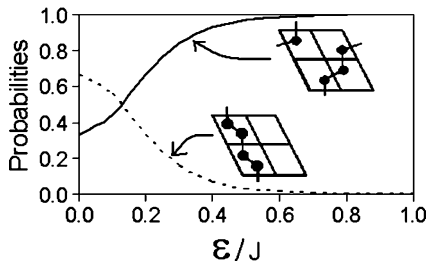

Fig. 17. Probabilities of classes (- - -) 0 and (—) 12 on 2×2 hexagonal lattice at $kT/J = 0.1$, $T/T_c(0) = 0.066$.

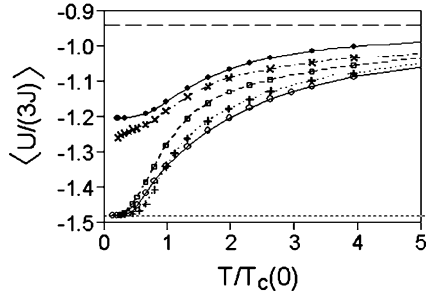

Fig. 18. Energy of 3×3 hexagonal lattice. Values of ε: (○) 0, (- -+- -) $3J$, (–□–) $6J$, (-×-) $9J$, and (●) infinity.

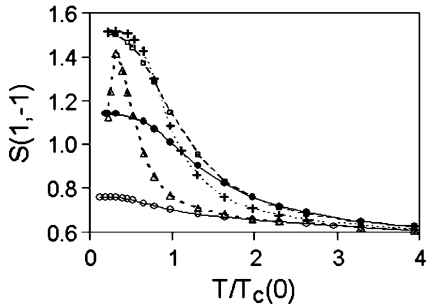

Fig. 19. Structure factor of 3×3 hexagonal lattice. Values of ε: (○) 0, (-Δ-) J, (- -+- -) $3J$, (□) $6J$, and (●) infinity.

There are three classes that have ten bonds, corresponding to the minimum 3×3 energy, so those three classes are dominant at low temperature and fields from 0 to about $7J$. Figure 20 shows probabilities of those classes at $kT/J = 0.5$ ($T/T_c(0) = 0.33$). One configuration from each class (each contains 18 configurations) is shown in Fig. 21. At zero field the three classes are equally probable. Larger fields select class 2439 which has zig-zag bond chains in the field direction. Unlike the 2×2 lattice, still higher fields spread probability to a mix of higher-energy classes (no one of which has probability greater than 0.07), resulting in the higher-energy plateau seen in Fig. 18 at infinite field and $T/T_c(0)$ less than about 0.5. The transition from low- to high-field probability distribution occurs over the ε range 6–$10J$. It is likely that similar probability shifts, over the same range of field strength but within a much larger space of configurations, explain the low-temperature high-field plateau in Fig. 12.

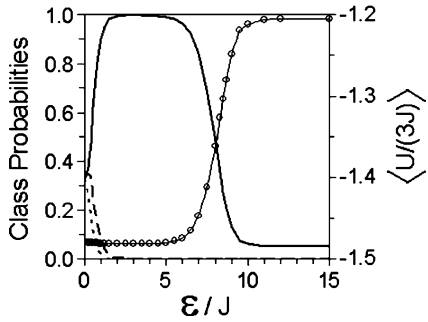

Fig. 20. Probabilities of maximum-bond classes on 3×3 hexagonal lattice. $kT/J = 0.5$, $T/T_c(0) = 0.33$. Class (—) 2439, (- - -) 2, (– – –)69. Energy (–○–) is on the right-hand ordinate.

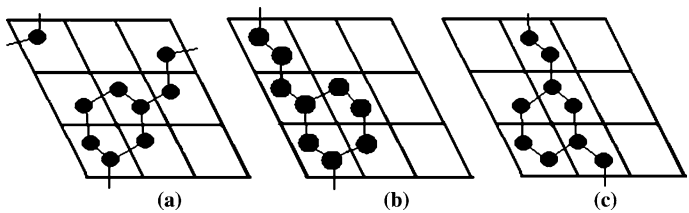

Fig. 21. Configurations from the maximum-bond classes of the 3×3 hexagonal lattice. (a) class 2439 configuration 27385, (b) class 2 configuration 2, (c) class 69 configuration 201.

8. CONCLUSIONS

In the driven lattice gas with Metropolis rates, and for the orientations and lattices studied, a strong field prevents transition to an ordered low-temperature state except when the field is perpendicular to a bond direction. Qualitatively, that may be understood in terms of stability of an interface between high- and low-density areas on the lattice. Unless the field is perpendicular to one of the bond directions, a well-ordered interface cannot be stable under a strong field, which would drive particles out of the interface. On the triangular lattice, with its six-fold site coordination, an interface along the [11] field and perpendicular to the $[1, -1]$ bond direction would still be susceptible to field-driven hops in the [01] and [10] directions. This simple observation may explain the absence of ordered states for most field orientations, but does not explain the states observed at high field and low temperature on hexagonal and triangular lattices.

When the field is perpendicular to a bond direction, then under an infinite field single-strip states have been observed on the square

lattice only. The disordered nature of the low-temperature configurations is strongly system-size dependent on the triangular lattice but independent of hexagonal lattice size. That is understandable on the hexagonal lattice because the strips that appear at low temperature, oriented along the field, are narrow. The broad [11] clustering seen on the triangular lattice at low temperature is impossible on truly small lattices because the stepped [11] interface limits the number of bonds. Even on the largest triangular lattices studied, however, the effect of system size on energy is huge at low temperature and the present work has not extrapolated to triangular lattices of infinite size.

Under low-strength fields both hexagonal and triangular lattice configurations align with the field over an intermediate temperature range, then freeze to the equilibrium-like solid at lower temperature. Stronger fields shift the structure-factor peak toward low temperature, leading to a disordered low-temperature state for fields greater than about $9J$. Solution of the 3×3 hexagonal-lattice master equation at low temperature shows the progression, with increasing field strength, from a normal frozen state to a field-aligned state and then, at about $9J$, to a disordered partially aligned state.

Two combinations of lattice and field orientation, [10] field on hexagonal and [11] field on triangular lattices, lead to steady states that may show phase transitions as functions of temperature and field strength. Some properties of energy and structure factors suggest that phase transitions occur. Energies drop from high-temperature near-disordered values to low-temperature plateaus and show inflections that correspond to weak heat-capacity maxima. Structure factor peaks indicate anisotropy along the field. Both Monte Carlo and exact small-lattice results show an abrupt change in the low-temperature states as field strength increases on the hexagonal lattice.

However, phase transitions should be signaled by singular dependence of properties on control parameters such as temperature and field strength, and no singularities have been shown here. Exact results on small hexagonal lattice can only suggest phase transitions. Anisotropic density inhomogeneity (e.g., Fig. 5) may show interfaces and phase coexistence on the triangular lattice but interpretation is complicated by strong dependence on system size at low temperature. The maximum entropy mean field method explicitly locates coexisting states and their critical points but the predicted critical temperatures appear to match simulations only in the well-known case of a [10] field on the square lattice. That the field raises the critical temperature is a striking feature of the square-lattice DLG. The present data with the present methods do not suffice to locate phase coexistence and critical temperatures for the triangular and hexagonal lattices.

ACKNOWLEDGMENTS

Computing resources were provided by the Visualization and Digital Imaging Laboratory of the University of Minnesota Duluth (UMD), the Minnesota Supercomputing Institute, and the UMD Department of Chemistry. K. S. C. Kumaran's help with the exact master equation method was indispensable.

REFERENCES

1. S. Katz, J. L. Lebowitz, and H. Spohn, Phase transitions in stationary nonequilibrium states of model lattice systems, *Phys. Rev. B* **28**(3):1655–1658 (1983).
2. S. Katz, J. L. Lebowitz, and H. Spohn, Nonequilibrium steady states of stochastic lattice gas models of fast ionic conductors, *J. Stat. Phys.* **34**(3/4):497–537 (1984).
3. B. Schmittmann and R. K. P. Zia, Statistical mechanics of driven diffusive systems, *Phase Transitions and Critical Phenomena*, Vol. 17. C. Domb and J. L. Lebowitz, eds. (Academic Press, London, 1995).
4. J. Marro and R. Dickman, *Nonequilibrium Phase Transitions in Lattice Models* (Cambridge University Press, Cambridge, 1999).
5. R. K. P. Zia, L. B. Shaw, B. Schmittmann, and R. J. Astalos, Contrasts between equilibrium and non-equilibrium steady states: Computer aided discoveries in simple lattice gases, *Comp. Phys. Comm.* **127**:23–31 (2000).
6. D. C. Mattis, *The Theory of Magnetism II: Thermodynamics and Statistical Mechanics* (Springer, Berlin, 1985), p. 100.
7. M. E. J. Newman and G. T. Barkema, *Monte Carlo Methods in Statistical Physics* (Clarendon Press, Oxford, 1999).
8. W. H. Press, S. A. Teukolsky, W. T. Vetterling, and B. P. Flannery, *Numerical Recipes in C: The Art of Scientific Computing*, 2nd ed. (Cambridge University Press, Cambridge, 1992).
9. W. Gropp, E. Lusk, and A. Skjellum, *Using MPI: Portable Parallel Programming with the Message-Passing Interface*, 2nd ed. (MIT Press, Cambridge MA, 1999).
10. A. Srinivasan, D. M. Ceperley, and M. Mascagni, Random number generators for parallel applications, in *Monte Carlo Methods in Chemical Physics*, D. M. Ferguson, J. I. Siepmann and D. G. Truhlar, eds, *Advances in Chemical Physics* Series, **105** (John Wiley and Sons, New York, 1999) pp. 13–36.
11. D. P. Landau and K. Binder, *A Guide to Monte Carlo Simulations in Statistical Physics* (Cambridge University Press, Cambridge, 2000).
12. J. L. Vallés and J. Marro, Nonequilibrium phase transitions in stochastic lattice systems: Influence of the hopping rates, *J. Stat. Phys.* **43**(3/4):441–461 (1986).
13. J. L. Vallés and J. Marro, Nonequilibrium second-order phase transitions in stochastic lattice systems: a finite-size scaling analysis in two dimensions, *J. Stat. Phys.* **49**(1/2):89–119 (1987).
14. R. K. P. Zia, L. B. Shaw, and B. Schmittmann, Possible existence of an extraordinary phase in the driven lattice gas, *Physica A* **279**:60–68 (2000).
15. R. Dickman, Mean-field theory of the driven diffusive lattice gas, *Phys. Rev. A* **38**:2588–2593 (1988).
16. N. C. Pesheva, *A Mean-Field Method For Driven Diffusive Systems Based On Maximum Entropy Principle*, Virginia Polytechnic Institute and State University, Ph.D. Thesis, UMI 9000639 (1989).

17. N. C. Pesheva, Y. Shnidman, and R. K. P. Zia, A maximum entropy mean field method for driven diffusive systems, *J. Stat. Phys.* **70**(3/4):737–771 (1993).
18. M. Q. Zhang, Exact results on the steady state of a hopping model, *Phys. Rev. A* **35**(5):2266–2275 (1987).
19. Q. Zhang, *Nonequilibrium Steady States of a Stochastic Model System*, Rutgers, the State University of New Jersey, Ph.D. Thesis, UMI 8803528 (1987).
20. K. S. C. Kumaran, *Nonequilibrium Steady States of the Lattice Gas*, University of Minnesota, M.S. Thesis (2004).
21. Wolfram Research Inc, *Mathematica*, Version 5.0, Champaign, IL (2003).